AFRL-RX-WP-JA-2015-0129

LOW-DENSITY, REFRACTORY MULTI-PRINCIPAL ELEMENT ALLOYS OF THE Cr–Nb–Ti–V–Zr SYSTEM: MICROSTRUCTURE AND PHASE ANALYSIS (POSTPRINT)

O.N. Senkov, S.V. Senkova, C. Woodward, and D.B. Miracle
AFRL/RXCM

APRIL 2014
Interim Report

AIR FORCE RESEARCH LABORATORY
MATERIALS AND MANUFACTURING DIRECTORATE
WRIGHT-PATTERSON AIR FORCE BASE OH 45433-7750
AIR FORCE MATERIEL COMMAND
UNITED STATES AIR FORCE

NOTICE AND SIGNATURE PAGE

Using Government drawings, specifications, or other data included in this document for any purpose other than Government procurement does not in any way obligate the U.S. Government. The fact that the Government formulated or supplied the drawings, specifications, or other data does not license the holder or any other person or corporation; or convey any rights or permission to manufacture, use, or sell any patented invention that may relate to them.

Qualified requestors may obtain copies of this report from the Defense Technical Information Center (DTIC) (http://www.dtic.mil).

AFRL-RX-WP-JA-2015-0129 HAS BEEN REVIEWED AND IS APPROVED FOR PUBLICATION IN ACCORDANCE WITH ASSIGNED DISTRIBUTION STATEMENT.

//Signature//

MICHEAL E. BURBA, Project Engineer
Metals Branch
Structural Materials Division

//Signature//

DANIEL J. EVANS, Chief
Metals Branch
Structural Materials Division

//Signature//

ROBERT T. MARSHALL, Deputy Chief
Structural Materials Division
Materials And Manufacturing Directorate

This report is published in the interest of scientific and technical information exchange and its publication does not constitute the Government's approval or disapproval of its ideas or findings.

REPORT DOCUMENTATION PAGE

Form Approved
OMB No. 0704-0188

1. REPORT DATE *(DD-MM-YY)*	2. REPORT TYPE	3. DATES COVERED *(From - To)*
April 2014	Interim	19 March 2014 – 31 March 2014

4. TITLE AND SUBTITLE
LOW-DENSITY, REFRACTORY MULTI-PRINCIPAL ELEMENT ALLOYS OF THE Cr–Nb–Ti–V–Zr SYSTEM: MICROSTRUCTURE AND PHASE ANALYSIS (POSTPRINT)

5a. CONTRACT NUMBER
In-house

5b. GRANT NUMBER

5c. PROGRAM ELEMENT NUMBER
62102F

6. AUTHOR(S)
O.N. Senkov, S.V. Senkova, C. Woodward, and D.B. Miracle

5d. PROJECT NUMBER
4349

5e. TASK NUMBER

5f. WORK UNIT NUMBER
X0W6

7. PERFORMING ORGANIZATION NAME(S) AND ADDRESS(ES)

AFRL/RXCM
2941 Hobson Way
Bldg 654, Rm 136
Wright-Patterson AFB, OH 45433

8. PERFORMING ORGANIZATION REPORT NUMBER

9. SPONSORING/MONITORING AGENCY NAME(S) AND ADDRESS(ES)

Air Force Research Laboratory
Materials and Manufacturing Directorate
Wright-Patterson Air Force Base, OH 45433-7750
Air Force Materiel Command
United States Air Force

10. SPONSORING/MONITORING AGENCY ACRONYM(S)
AFRL/RXCM

11. SPONSORING/MONITORING AGENCY REPORT NUMBER(S)
AFRL-RX-WP-JA-2015-0129

12. DISTRIBUTION/AVAILABILITY STATEMENT
Distribution Statement A. Approved for public release; distribution unlimited.

13. SUPPLEMENTARY NOTES
Journal article published in *Acta Materialia* 61 (2013) 1545-1557. © 2012 Acta Materialia Inc. Published by Elsevier Ltd. The U.S. Government is joint author of the work and has the right to use, modify, reproduce, release, perform, display or disclose the work. This report contains color. The final publication is available at http://dx.doi.org/10.1016/j.actamat.2012.11.032

14. ABSTRACT

The crystal structure, microstructure, density and Vickers hardness of four multi-principal element alloys, NbTiVZr, $NbTiV_2Zr$, CrNbTiZr, and CrNbTiVZr, are reported. The characteristics of these potential new high-temperature structural alloys are explored. The alloys were prepared by vacuum arc melting followed by hot isostatic pressing (at 1200 °C, 207 MPa for 1 h) and homogenization annealing (at 1200 °C for 24 h). The alloys have densities of 6.52, 6.34, 6.67 and 6.57 g cm−3, and Vickers microhardness values of 3.29, 2.99, 4.10 and 4.72 GPa, respectively. The NbTiVZr alloy is essentially a single-phase alloy consisting of a coarse-grained disordered body-centered cubic (bcc) phase with fine, submicron-size precipitates inside the grains. The $NbTiV_2Zr$ alloy contains three disordered bcc phases. The CrNbTiZr and CrNbTiVZr alloys contain a disordered bcc phase and an ordered Laves phase. The lattice parameters and compositions of the identified phases are reported. The experimental data are compared with the results of the thermodynamic modeling of non-equilibrium and equilibrium phases in these alloys.

15. SUBJECT TERMS
refractory alloys, crystal structure, microstructure, CALPHAD

16. SECURITY CLASSIFICATION OF:			17. LIMITATION OF ABSTRACT:	18. NUMBER OF PAGES	19a. NAME OF RESPONSIBLE PERSON (Monitor)
a. REPORT	b. ABSTRACT	c. THIS PAGE			Micheal E. Burba
Unclassified	Unclassified	Unclassified	SAR	16	19b. TELEPHONE NUMBER *(Include Area Code)* (937) 255-9795

Available online at www.sciencedirect.com

SciVerse ScienceDirect

Acta Materialia 61 (2013) 1545 1557

Acta MATERIALIA

www.elsevier.com/locate/actamat

Low-density, refractory multi-principal element alloys of the Cr Nb Ti V Zr system: Microstructure and phase analysis

O.N. Senkov*, S.V. Senkova, C. Woodward, D.B. Miracle

Air Force Research Laboratory, Materials and Manufacturing Directorate, Wright Patterson AFB, OH 45433, USA

Received 28 August 2012; received in revised form 16 November 2012; accepted 18 November 2012
Available online 19 December 2012

Abstract

The crystal structure, microstructure, density and Vickers hardness of four multi principal element alloys, NbTiVZr, $NbTiV_2Zr$, CrNbTiZr, and CrNbTiVZr, are reported. The characteristics of these potential new high temperature structural alloys are explored. The alloys were prepared by vacuum arc melting followed by hot isostatic pressing (at 1200 °C, 207 MPa for 1 h) and homogenization annealing (at 1200 °C for 24 h). The alloys have densities of 6.52, 6.34, 6.67 and 6.57 g cm^{-3}, and Vickers microhardness values of 3.29, 2.99, 4.10 and 4.72 GPa, respectively. The NbTiVZr alloy is essentially a single phase alloy consisting of a coarse grained disordered body centered cubic (bcc) phase with fine, submicron size precipitates inside the grains. The $NbTiV_2Zr$ alloy contains three disordered bcc phases. The CrNbTiZr and CrNbTiVZr alloys contain a disordered bcc phase and an ordered Laves phase. The lattice parameters and compositions of the identified phases are reported. The experimental data are compared with the results of the thermodynamic mod eling of non equilibrium and equilibrium phases in these alloys.

Keywords: Refractory alloys; Crystal structure; Microstructure; CALPHAD

1. Introduction

Multi-principal element alloys, also known as high entropy alloys (HEAs) because of their high entropy of mixing of alloying elements, have recently come to the attention of the scientific community due to some interesting and unexpected microstructures and properties [1 3]. These alloys consist of four, five or even more alloying elements at near-equiatomic concentrations. In spite of high alloying, only disordered solid-solution phases, often with face-centered cubic (fcc) and/or body-centered cubic (bcc) crystal structures, form in many of these alloys after solidification. This is explained by the high entropy of formation, which effectively reduces the Gibbs free energy of these disordered phases relative to ordered intermetallics, especially at high temperatures. However, in some cases intermetallic phases still form in HEAs after heat treatment or thermo-mechanical treatment. Even if ordered intermetallic phases are present, the major phases in these alloys are disordered solid solution phases. Intermetallic phase formation in HEAs is thought to be favored by large atomic size mismatch, as well as large, negative enthalpies of mixing of the alloying elements [4,5].

Recently, a HEA approach has been applied to produce several new refractory alloys with promising combinations of room temperature and elevated temperature mechanical properties and oxidation resistance [6 11]. These are MoNbTaW, MoNbTaVW [6,7], HfNbTaTiZr [8,9] and $CrMo_{0.5}NbTa_{0.5}TiZr$ [10,11]. The high entropy of mixing and similar atomic radii of the alloying elements resulted in the formation of a single-phase bcc crystal structure in the first three alloys. However, the presence of Cr with an atomic radius that is much smaller than the atomic radii of other elements in the fourth alloy caused additional formation of a minor fcc Laves phase [10]. These refractory alloys have rather high densities, from 8.2 g cm^{3} for $CrMo_{0.5}NbTa_{0.5}TiZr$ to 13.8 g cm^{3} for MoNbTaW,

* Corresponding author. Tel.: +1 937 255 4064; fax: +1 937 656 7292.
E mail address: oleg.senkov@wpafb.af.mil (O.N. Senkov).

1359 6454/$36.00 © 2012 Acta Materialia Inc. Published by Elsevier Ltd. All rights reserved.
http://dx.doi.org/10.1016/j.actamat.2012.11.032

which may be satisfactory for potential applications of stationary structures that do not suffer from high weight. Since the aerospace industry demands low-density metallic alloys for high-temperature load-bearing structures and thermal protection systems, there is a clear rationale for exploring HEAs composed of constituents with high melting temperatures and reduced densities. Therefore, the goal of the current work was to produce refractory HEAs with densities below 7.0 g cm ^{3}, which could operate at temperatures as high as 1000 °C. To achieve this goal, low-density refractory elements, V (ρ_V 6.11 g cm ^{3}), Zr (ρ_{Zr} 6.51 - g cm ^{3}), Cr (ρ_{Cr} 7.14 g cm ^{3}), Nb (ρ_{Nb} 8.57 g cm ^{3}) and Ti (ρ_{Ti} 4.51 g cm ^{3}) were selected to produce four alloys: NbTiVZr, $NbTiV_2Zr$, CrNbTiZr and CrNbTiVZr. The microstructure and phase compositions of these alloys are described here; the mechanical properties will be reported in a subsequent paper [12].

2. Experimental procedures

The Cr Nb Ti V Zr alloys were prepared by vacuum arc melting of nominal mixtures of the corresponding elements. Titanium and zirconium were in the form of 3.175 mm diameter slugs with purities of 99.99 and 99.95%, respectively. Niobium and tantalum were in the form of 1.0 and 2.0 mm wires, and their purities were 99.95 and 99.9%, respectively. Chromium was in the form of 10 100 mm^3 pieces, with a purity of 99.95%. Vanadium was in the form of chips, with a purity of 99.99%. Arc melting was conducted on a water-cooled copper plate. High-purity molten titanium was used as a getter for residual oxygen, nitrogen and hydrogen. To achieve a homogeneous distribution of elements in the alloys, each alloy was remelted five times, being flipped for each melt, and was in a liquid state for about 5 min during each melting event. The prepared cigar-shaped specimens were about 12 mm high, 30 mm wide and 100 mm long, and had shiny surfaces, indicating that there was no oxidation during the vacuum arc melting. The actual alloy compositions determined by inductively coupled plasma-optical emission spectroscopy are given in Table 1. The produced alloys were hot isostatically pressed (HIPed) at 1200 °C and 207 MPa for 2 h, then homogenized by annealing at 1200 °C for 24 h in high-purity argon. During HIP and annealing, the samples were covered with Ta foil to minimize oxidation. The cooling rate after annealing was 10 °C min ^{1}. The crystal structure was identified with the use of an X-ray diffractometer using Cu K_α radiation and a 2Θ scattering range of 10 140°.

Alloy density was measured with an AccuPyc 1330 V1.03 helium pycnometer. The pycnometer cell volume was 12.2284 cm^3, the sample weight was ~10 g, measured to an accuracy of ±0.0001 g, and the sample volume was determined to an accuracy of ±0.0001 cm^3 by measuring the free volume of the loaded cell using helium gas and 10 purges. Vickers microhardness was measured on polished cross-section surfaces using a 136° Vickers diamond pyramid under a 500 g load applied for 20 s. The microstructure was analyzed by scanning electron microscopy (SEM) using a Quanta 600F scanning electron microscope (FEI, North America NanoPort, Hillsboro, OR) equipped with backscatter electron (BSE), energy-dispersive X-ray spectroscopy (EDS) and electron backscatter diffraction (EBSD) detectors.

Thermodynamic modeling of the non-equilibrium solidification (Scheil model) and equilibrium phase diagrams of the studied alloys was conducted using the Pandat version 8.0 software [13] employing the PanTi thermodynamic database developed by Computherm, LLC.

3. Results

3.1. Density and hardness of the homogenized alloys

The produced refractory alloys, NbTiVZr, $NbTiV_2Zr$, CrNbTiZr and CrNbTiVZr, have relatively low densities, of ρ 6.52 ± 0.01, 6.34 ± 0.01, 6.67 ± 0.01 and 6.57 ± 0.01 g cm ^{3}, respectively. Using the densities of pure elements and the alloy compositions (Table 1), one can estimate the density, ρ_{mix}, of disordered solid solutions of the same compositions using the rule of mixtures:

$$\rho_{mix} = \frac{\sum c_i A_i}{\sum \frac{c_i A_i}{\rho_i}} \quad (1)$$

Here c_i, A_i and ρ_i are the concentration, atomic weight and density of element i. The calculated ρ_{mix} values are very close to the densities of homogenized alloys (see Table 1). A similar observation has been previously reported for other high entropy alloys [6,8,10]. The Vickers microhardness, Hv, was measured in 20 randomly selected locations of each alloy and the average values are given in Table 1 Among the three quaternary alloys, $NbTiV_2Zr$ has the lowest hardness (Hv 2.99 ± 0.03 GPa) and CrNbTiZr the highest (Hv 4.10 ± 0.04 GPa), while NbTiVZr has Hv 3.29 ± 0.03 GPa. The five-element alloy, CrNbTiVZr, has Hv 4.72 ± 0.05 GPa. For comparison,

Table 1
Chemical compositions (in at.%), density, ρ, and Vickers microhardness, H_v, of the alloys studied in this work.

Alloy	Cr	Nb	Ti	V	Zr	ρ (g cm ^{3})	ρ_{mix} (g cm ^{3})	H_V (GPa)
NbTiVZr		28.3	24.5	23.0	24.2	6.52	6.50	3.29 ± 0.03
$NbTiV_2Zr$		22.6	19.4	37.2	20.8	6.34	6.38	2.99 ± 0.03
CrNbTiZr	24.6	26.7	23.9		24.8	6.67	6.70	4.10 ± 0.04
CrNbTiVZr	20.2	20.0	19.9	19.6	20.3	6.57	6.52	4.72 ± 0.05

the density and Vickers hardness of a high-strength Ni superalloy 718 are ρ 8.19 g cm ^{3} and Hv 3.6 GPa [14].

3.2. Crystal structure

An X-ray diffraction pattern of the NbTiVZr alloy is shown in Fig. 1a. The Braggs peaks are identified as belonging to a single phase with a bcc crystal structure and the lattice parameter a 332.5 pm. The absence of superlattice peaks indicates that this is a disordered bcc (A2) phase. An X-ray diffraction pattern of the $NbTiV_2Zr$ alloy is shown in Fig. 1b. The Braggs peaks are identified to belong to three phases, which have disordered bcc crystal structures (bcc1, bcc2 and bcc3), with lattice parameters a_1 345.8 pm, a_2 317.4 pm and a_3 323.5 pm, respectively.

An X-ray diffraction pattern of the CrNbTiZr alloy is shown in Fig. 1c. The Braggs peaks are identified as belonging to two phases. One is a disordered bcc phase, with the lattice parameter a 336.5 pm. Another is an ordered Laves (C15) phase, with an fcc crystal structure and the lattice parameter a 725.5 pm. An X-ray diffraction pattern of the CrNbTiVZr alloy is shown in Fig. 1d. The Braggs peaks are identified as belonging to two phases, with disordered bcc (A2) and ordered fcc (Laves phase C15) crystal structures. The lattice parameter of the bcc phase is a 330.1 pm and that of the Laves phase is a 730.8 pm.

3.3. Microstructure

3.3.1. NbTiVZr

Representative SEM backscatter images of the NbTiVZr alloy are shown in Fig. 2 and EBSD/EDS phase and composition maps are given in Fig. 3. The alloy consists of a matrix with large (~600 μm in diameter) grains and a composition close to that of the alloy. Spots about 20 30 μm in diameter, which look bright in BSE images (Fig. 2a) and dark in the secondary electron image mode (Fig. 3a) and have a total volume fraction of ~3 6%, are homogeneously distributed inside the matrix. EDS mapping shows that these spots are depleted of V (dark regions in Fig. 3c) and enriched with Zr (light regions in Fig. 3d). Additionally, submicron-sized second-phase particles are seen on the BSE images by their dark contrast (Fig. 2). These particles form characteristic chains, probably due to heterogeneous nucleation at dislocations and/or subgrain boundaries, and are often surrounded by bright-contrast shells (Fig. 2b). They are not seen on the secondary electron images (Fig. 3a). From Fig. 2a, it seems that these chains of second-phase particles are more common in the Zr-enriched regions. Spot EDS sampling indicates that the dark particles are enriched with V, while the bright regions surrounding the dark particles are enriched with Zr (Table 2). Unfortunately, the exact compositions of these dark particles and surrounding bright regions could not be determined due to their small dimensions. Additional TEM studies are required to determine the crystal structure and chemistry of these second-phase particles. The EBSD phase analysis identifies the presence of a bcc phase only in this alloy (Fig. 3b).

3.3.2. $NbTiV_2Zr$

The $NbTiV_2Zr$ alloy has a rather complex microstructure (Fig. 4). Three constituents with different BSE contrasts (white, grey and dark) are clearly identified in the low-magnification BSE images (Fig. 4a and b). A higher-magnification image (Fig. 4c) resolves the more complex

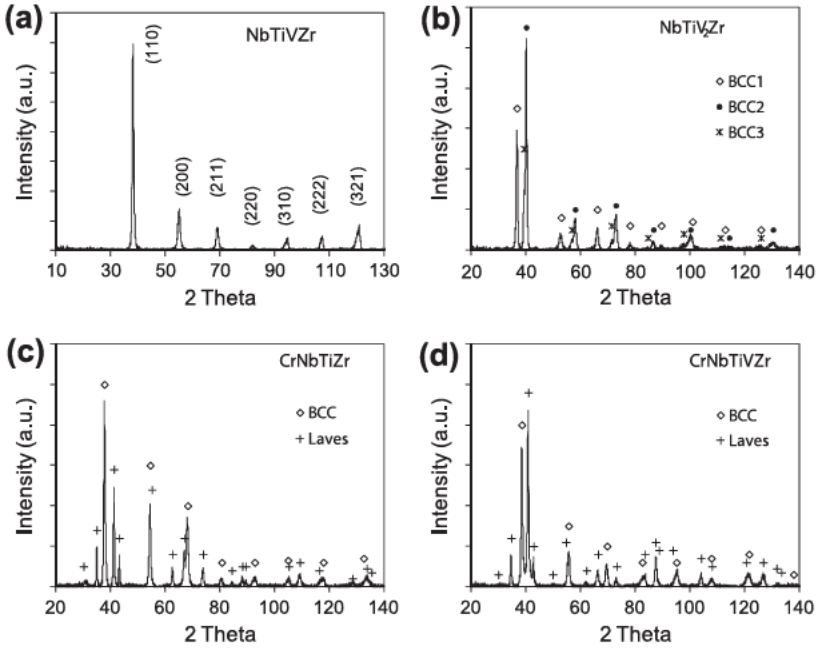

Fig. 1. X ray diffraction patterns from the annealed alloys: (a) NbTiVZr, (b) $NbTiV_2Zr$, (c) CrNbTiZr and (d) CrNbTiVZr.

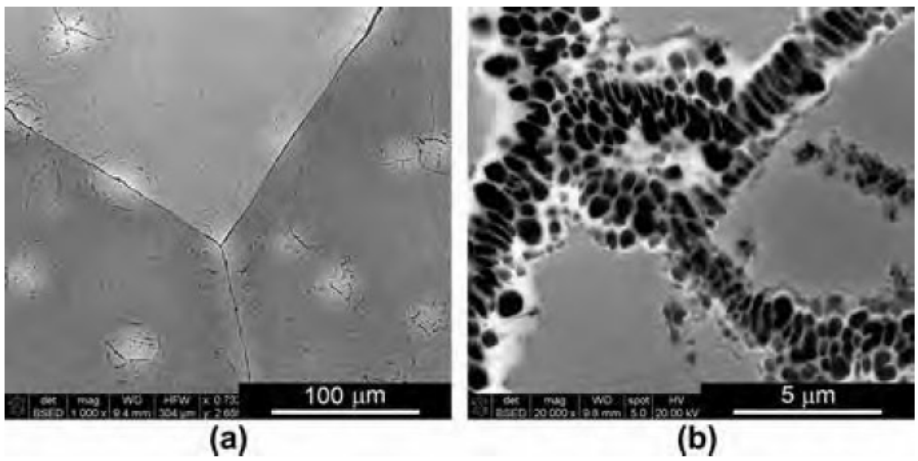

Fig. 2. SEM backscatter electron images of the grain structure and precipitates in the cast and homogenized NbVTiZr alloy.

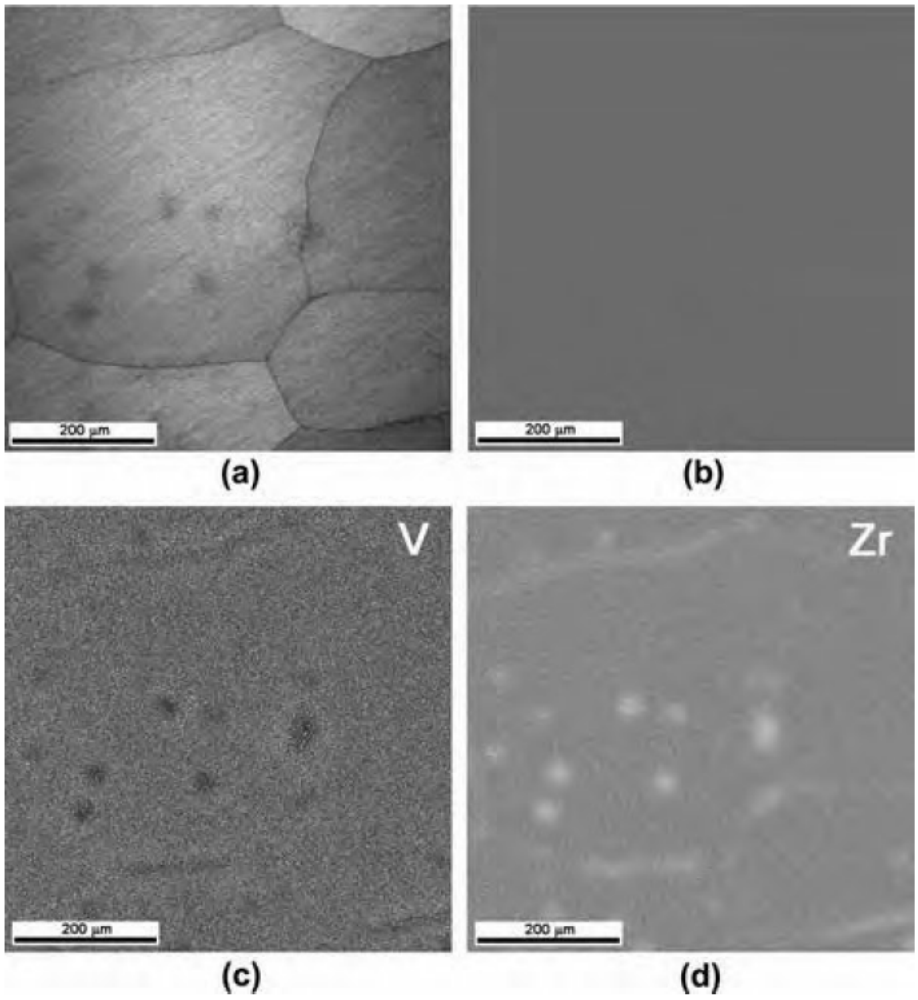

Fig. 3. EBSD/EDS data for the NbVTiZr alloy: (a) image quality, (b) phase map (grey is bcc, white is fcc) and (c and d) composition maps of (c) vanadium and (d) zirconium (lighter regions correspond to higher concentrations of the alloying elements).

structure of the grey regions, consisting of very fine precipitates of white and dark particles, as well as non-transformed grey regions. The total volume fractions of the white, non-transformed grey and dark phases are estimated to be $\sim 28 \pm 2$, 20 ± 5 and $52 \pm 4\%$, respectively. EDS analysis shows that the white regions are enriched with Zr and depleted of V, the grey regions are depleted of Zr, and the dark regions are enriched with V and depleted of

Table 2
Chemical composition (in at.%) of the NbVTiZr alloy constituents (see Fig. 2).

	Nb	Ti	V	Zr
Matrix (grey)	27.7	24.4	23.7	24.2
Black particles	22.1	20.5	38.9	18.5
White regions near particles	24.4	22.1	21.0	32.5

Table 3
Chemical composition (in at.%) of the NbV_2TiZr alloy constituents (see Fig. 4).

	Nb	Ti	V	Zr
White regions	21.4	19.2	10.7	48.6
Dark regions	23.2	19.7	48.2	8.9
Grey regions	23.8	19.7	42.5	14.0

Zr (Table 3). Among these three constituents, the composition of the grey regions is the closest to the alloy composition. A combined EBSD/EDS analysis clearly identifies that these three phases have bcc crystal structures (Fig. 5), in agreement with the X-ray diffraction data (Fig. 1b). The particles, which are enriched with Zr and depleted of V, have a grey color on the secondary electrons (SE) image (Fig. 5a), are dark on the V map (Fig. 5c), and are bright on the Zr map (Fig. 5d) and on the BSE images (Fig. 4). The particles slightly depleted of Zr are identified as light grey on the SE and V map images (Fig. 5a and c), dark on the Zr map (Fig. 5d) and grey on the BSE image (Fig. 4b). The phase depleted of Zr and enriched with V is located between the other two phases and is identified as being dark on the BSE image (Fig. 4b), bright on the SE and V map images (Fig. 5a and c), and very dark on the Zr map image (Fig. 5d). The comparison of the intensities of the X-ray peaks (Fig. 1b) and the volume fractions of the three phases suggests that the bcc2 phase (a_2 317.4 pm) is the major phase, with a volume fraction of $\sim 52 \pm 4\%$, and this is enriched with V and depleted of Zr. The bcc1 phase (a_1 345.8 pm) is the second major phase, which a volume fraction of $\sim 28 \pm 2\%$, and is enriched with Zr and depleted of V. The bcc3 phase (a_3 323.5 pm) has the volume fraction of $20 \pm 5\%$, is slightly depleted of Zr and has a composition (as well as a lattice parameter) that is very close to the volume-fraction average of the compositions (lattice parameters) of the bcc1 and bcc2 phases. This phase/composition analysis is also supported by the direct relationships between the lattice constants of the identified bcc phases and the concentration-averaged atomic radii of the alloying elements.

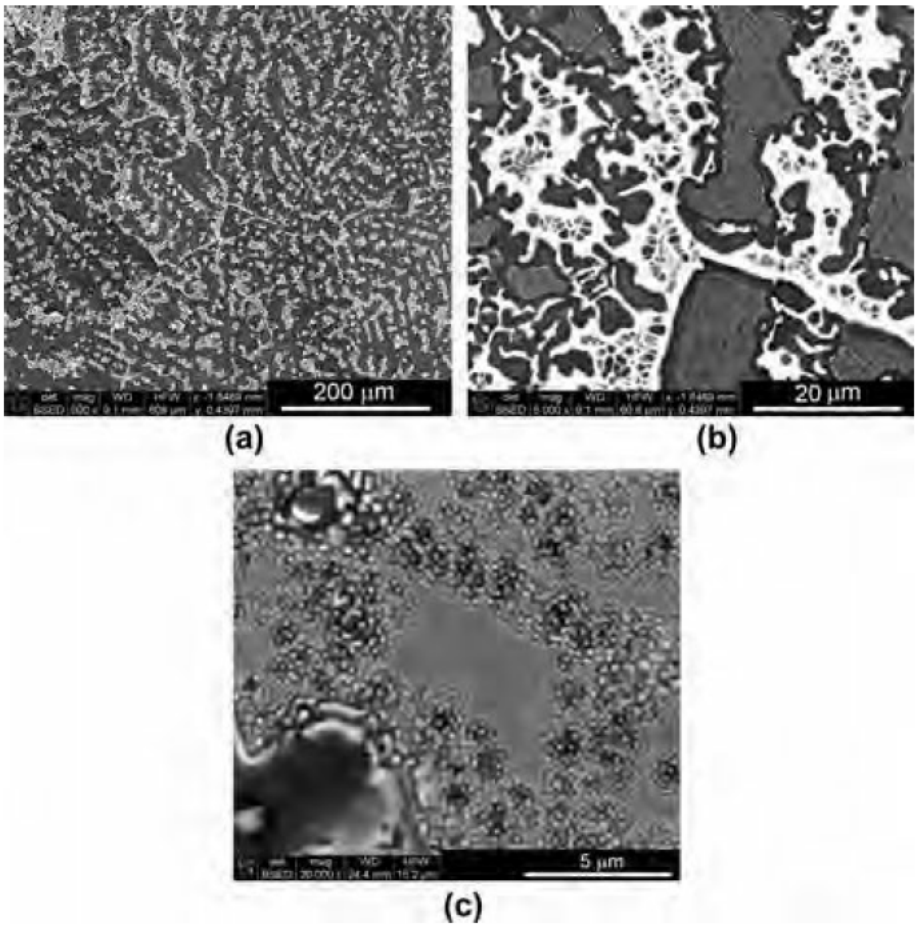

Fig. 4. SEM backscatter electron images of the microstructure in the cast $NbTiV_2Zr$ alloy in the homogenized condition.

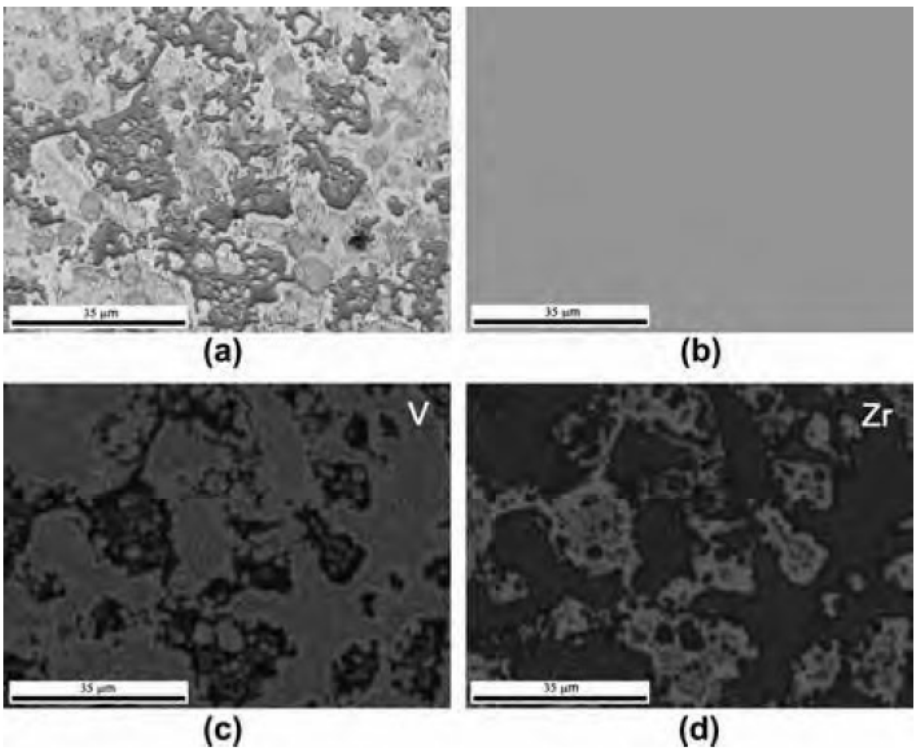

Fig. 5. EBSD/EDS data for the $NbTiV_2Zr$ alloy: (a) SEM image quality, (b) BCC phase map and (c and d) composition maps of (c) vanadium and (d) zirconium (lighter regions correspond to higher concentrations of the alloying elements).

Namely, large Zr atoms increase the lattice parameter of the bcc1 phase, while small V atoms reduce the lattice parameter of the bcc2 phase, relative to the bcc3 phase.

3.3.3. CrNbTiZr

A typical microstructure of homogenized CrNbTiZr is shown in Fig. 6. Two constituents, having bright and dark contrasts in the SEM backscatter conditions, are clearly identified. The average compositions of these regions, identified by EDS, are given in Table 4. The bright regions are enriched with Nb and Ti and have a low concentration of Cr. At the same time, dark regions are rich with Cr, the concentration being twice the average concentration in the alloy. A combined EBSD/EDS analysis shows (Fig. 7) that the Nb- and Ti-enriched regions have a bcc crystal structure. The volume fraction of these regions is estimated to be 65%. The Cr-rich regions have an fcc crystal structure and their volume fraction is 35%.

3.3.4. CrNbTiVZr

BSE images of the microstructure of this alloy are given in Fig. 8. Regions with three distinct colors bright, grey and dark grey can be identified. However, EDS and EBSD analyses show that the grey and darker regions have the same fcc crystal structure and their chemical compositions are identical (Fig. 9, Table 5). The different backscatter contrast in this case is probably due to different grain orientations. The volume fractions of the fcc and bcc phases are estimated to be 61 and 39%, respectively. The fcc phase is enriched with Cr and depleted of Ti, while the bcc phase is rich with both Nb and Ti (Table 5).

3.4. Thermodynamic modeling

Because phase diagrams for the studied alloys are unavailable, an attempt has been made in this work to model non-equilibrium phases produced in these alloys during non-equilibrium solidification and equilibrium phases presented at different temperatures. The phase modeling was conducted using the commercial thermodynamic software Pandat, version 8.0, and the PanTi thermodynamic database.

3.4.1. Non-equilibrium solidification

Non-equilibrium (NE) solidification kinetics of the studied alloys are shown in Fig. 10. The temperatures of start, T_L^{NE}, and completion, T_S^{NE}, of solidification and the estimated solid-phase volume fractions are shown in Table 6. The volume-averaged elemental concentrations in the solidified phases are given in Table 7. The solidification starts by the formation of a disordered bcc (A2-1) phase in all four alloys. An additional ordered Laves (C15) phase forms in the CrNbTiZr and CrNbTiVZr alloys, causing a noticeable change in the slopes of the respective solidification curves (see Fig. 10). A very small volume fraction (0.1 0.5%) of the secondary disordered bcc (A2-2) phase is formed at the end of solidification in the NbTiVZr, $NbTiV_2Zr$ and CrNbTiVZr alloys.

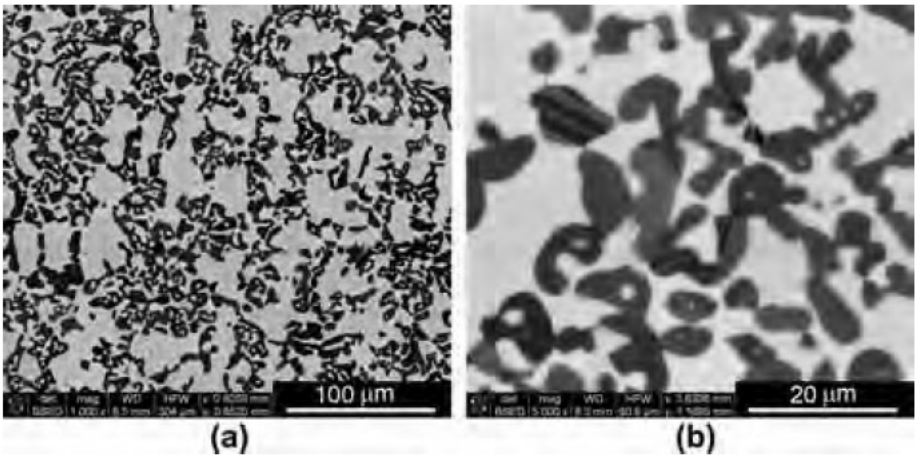

Fig. 6. SEM backscatter electron images of the microstructure in the cast CrNbTiZr alloy in the homogenized condition.

Table 4
Chemical composition (in at.%) of the CrNbTiZr alloy constituents (see Fig. 6).

	Cr	Nb	Ti	Zr
Bright regions	7.9	34.6	31.4	26.1
Dark regions	51.5	15.8	12.1	20.6

The NE solidification of NbTiVZr and $NbTiV_2Zr$ starts at $T_L^{NE} = 1760$ and 1717 °C, respectively, and is completed at $T_S^{NE} = 1207$ °C, which is the same for both alloys. After solidification, these Cr-free alloys do not contain intermetallic phases; only disordered bcc phases are present (see Tables 6 and 7). The NbTiVZr alloy is essentially a single-phase A2-1 structure, with elemental concentrations in this phase corresponding to the nominal alloy composition. $NbTiV_2Zr$ additionally contains a small amount (~0.5%) of the second A2-2 phase, which is enriched with V.

The CrNbTiZr alloy starts to solidify at the lowest temperature ($T_L^{NE} = 1572$ °C) and solidification is completed at the highest temperature ($T_S^{NE} = 1391$ °C) of all the alloys, providing the narrowest solidification range of $\Delta T = T_L^{NE} - T_S^{NE} = 181$ °C. After solidification, this alloy, in accord with the simulated results, consists of ~91% of the A2-1 phase and ~9% of the C15 phase. The A2-1 phase is slightly enriched with Nb and Ti and slightly depleted with Cr, while the C15 phase is enriched with Cr and Zr (Table 7). The CrNbTiVZr alloy starts to solidify at $T_L^{NE} = 1607$ °C and has a rather wide solidification range (ΔT 504 °C), similar to the quaternary alloys without Cr. After solidification, this alloy consists of essentially two phases, A2-1 and C15, with volume fractions of 95% and 4.5%, respectively. A small amount (0.5%) of a second A2-2 phase, mainly consisting of Zr, V and Cr, is also predicted in the CrNbTiVZr alloy.

3.4.2. Equilibrium phase diagrams

The calculated equilibrium phase diagrams of the studied alloys are given in Fig. 11. The reaction equations and phase transition temperatures are given in Table 8. Equilibrium solidification occurs in a much narrower range than NE solidification and results in formation of a disordered bcc (A2-1) phase in these alloys. With decreasing temperature, the A2-1 phase partially transforms into a C15 phase in CrNbTiZr and CrNbTiVZr, with solvus temperatures, T_s^{C15}, of 1363 and 1234 °C, respectively, and into a secondary disordered bcc (A2-2) phase in the NbTiVZr, $NbTiV_2Zr$ and CrNbTiVZr alloys, at $T_s^{A2-2} =$ 726, 843 and 671 °C, respectively. A disordered hexagonal phase (A3) is predicted to be present below $T_s^{A3} = 471$, 456, 535 and 440 °C in the NbTiVZr, $NbTiV_2Zr$, CrNbTiZr and CrNbTiVZr, alloys, respectively. Finally, complete transformation of the A2-1 phase into A2-2 and A3 phases occurs in the NbTiVZr, $NbTiV_2Zr$ and CrNbTiVZr alloys at 446, 426 and 433 °C, respectively.

The volume fractions and concentrations of the equilibrium phases at 600 and 400 °C are given in Tables 9 and 10, respectively. At 600 °C, the A2-1 phase is the major phase in the NbTiVZr and CrNbTiZr alloys, and A2-2 is the major phase in the other two alloys. In the V-containing alloys, A2-1 is enriched with Ti and Zr, while the A2-2 phase is enriched with Nb and V. In CrNbTiZr, which does not contain A2-2, the A2-1 phase is enriched with Nb and Ti. The intermetallic C15 phase is based on Cr and Zr, with a stoichiometry very near Cr_2Zr.

The phase compositions change drastically when the temperature decreases to 400 °C. Here, the A2-1 phase is present only in CrNbTiZr, which mainly consists of Nb (93.9 at.%). The A2-2 phase, enriched with Nb and V, becomes the major phase in the Cr-free alloys. The hexagonal A3 phase, enriched with Ti and Zr, is present in all four alloys, and the Cr-containing alloys also contain the C15 phase (Cr_2Zr).

4. Discussion

It is often stated that the high entropy of mixing in multi-principle element alloys stabilizes solid solutions with

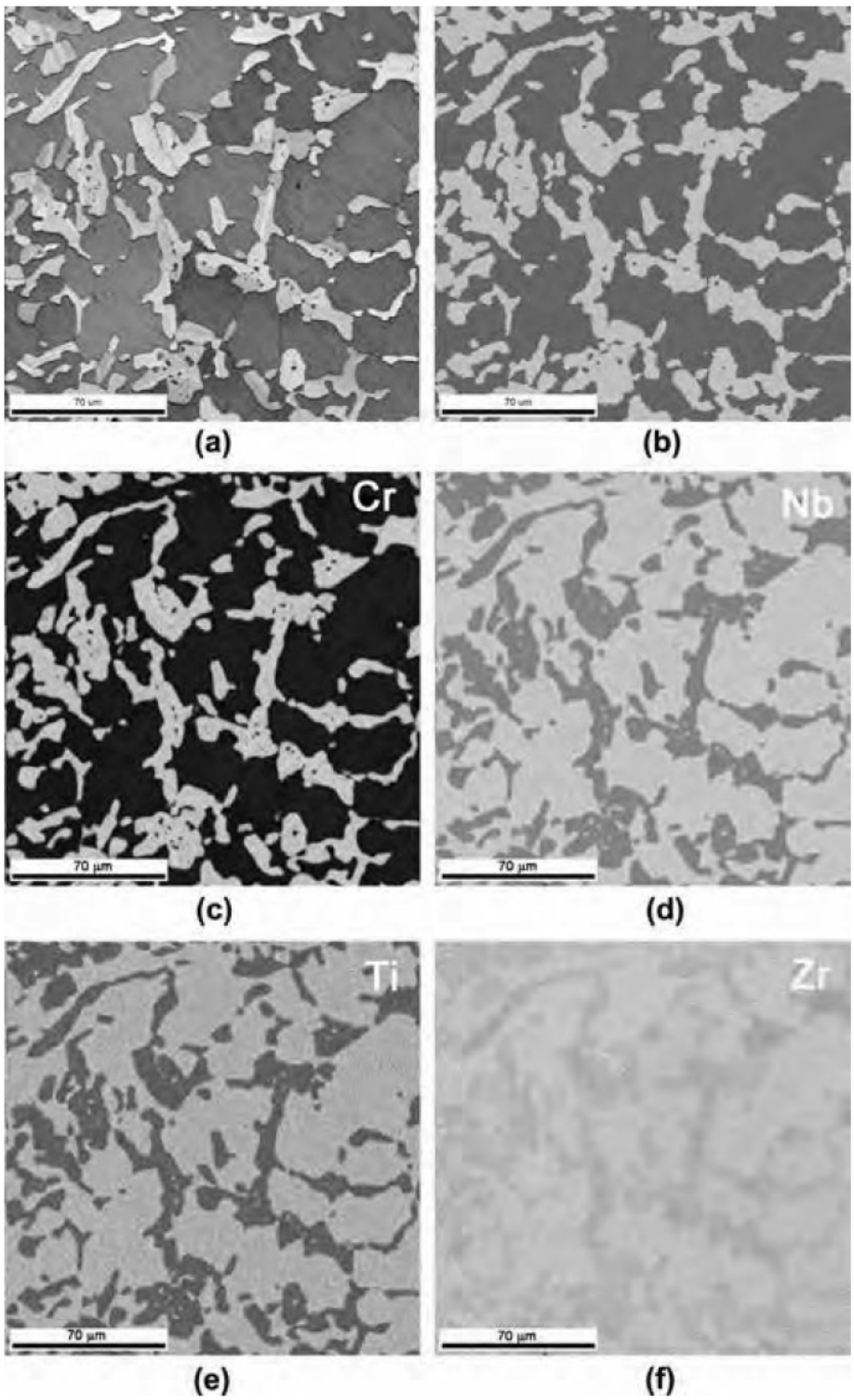

Fig. 7. EBSD/EDS data for the CrNbTiZr alloy: (a) image quality, (b) phase map (bcc is dark, fcc is bright) and (c f) composition maps of (c) chromium, (d) niobium, (e) titanium and (f) zirconium (lighter regions correspond to higher concentrations of the alloying elements).

a simple crystal structure relative to competing ordered intermetallic phases [2 4]. The present thermodynamic analysis shows that, after rapid (non-equilibrium) solidification, the NbTiVZr and $NbTiV_2Zr$ alloys consist of disordered bcc solid solutions, while the Cr-containing alloys, CrNbTiZr and CrNbTiVZr, additionally contain a small amount of an intermetallic Laves phase. In the equilibrium solid-state condition, the NbTiVZr and $NbTiV_2Zr$ alloys are single-phase disordered bcc solid solutions at temperatures above 726 and 843 °C, respectively, while the Laves phase formation narrows the equilibrium single-phase bcc range in the Cr-containing alloys by shifting it to higher

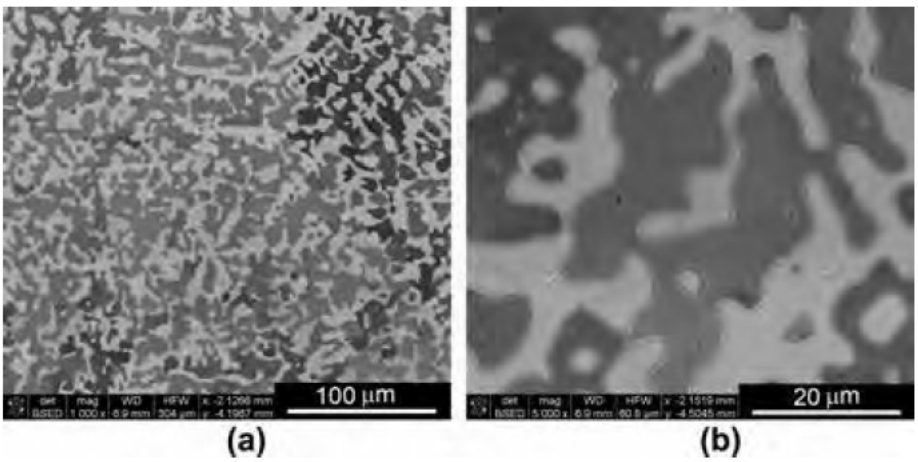

Fig. 8. SEM backscatter electron images of the microstructure in the cast CrNbTiVZr alloy in the homogenized condition.

temperatures, i.e. above 1363 and 1234 °C for CrNbTiZr and CrNbTiVZr, respectively (see Fig. 11). This, along with the present microstructural observations, seems to support the basic premise of high entropy alloys to stabilize disordered solid solution phases by lowering their Gibbs free energy through an increased entropy term at high temperatures and by slowing down equilibrium phase transformations due to sluggish diffusion at lower temperatures [2]. However, of the 10 binary phase diagrams that can be formed from the five elements in the present alloys, six show complete solid solubility at high temperatures. Two of these (Cr V, Nb V) have only one crystal phase with a bcc structure, and disordered bcc and hexagonal close-packed (hcp) phases form in the others (Nb Ti, Nb Zr, Ti V, Ti Zr). These two phases are both present at room temperature in all but the Ti Zr system, where the high-temperature bcc solid solution transforms completely to the hcp solid solution across the full composition range of the binary system. The elements in the present systems thus show a predisposition toward extensive solid solutions of disordered phases, even in binary systems. The present work therefore neither supports nor contradicts the basic idea behind high entropy alloys of stabilizing disordered solid solutions. The purpose of this work is to explore the characteristics of potential new high-temperature structural metals, and is not to explore the degree to which intermetallic phases may be avoided in multi-principle element alloys.

In the remaining four binary systems (Cr Nb, Cr Ti, Cr Zr and V Zr), a single ordered intermetallic phase forms with a stoichiometry of Cr_2X or V_2X. In each instance, the phase formed is a Laves phase with the cubic C15 structure at high temperature. In all but the V_2Zr phase, the C15 structure transforms at lower temperatures to the C14 or C36 ordered hexagonal structure. The most stable of these Laves phases is Cr_2Nb, which forms at 1770 °C. In addition to factors that include the bond enthalpies between atoms, the small atomic radius of Cr (r_{Cr} 128 pm) relative to the atomic radii of other alloying elements (r_{Nb} 142.9 pm, r_{Ti} 141.8 pm, r_V 134.0 pm, r_{Zr} 155.1 pm) may favor formation of the ordered Laves phase by reducing the elastic energy of the competing solid solution phases. Indeed, in the present alloys, Cr preferentially couples with Zr, which has the largest atomic radius among the elements of the studied alloys.

In the CrNbTiZr and CrNbTiVZr alloys, the modeled equilibrium diagrams show that the Laves phase is stable at room temperature, but that it is completely dissolved above about 1300 °C (Fig. 11). This gives the possibility of designing heat-treatable alloys with microstructures that may be controlled through dissolution and subsequent aging at lower temperatures. It remains to be seen if the nucleation and growth of the C15 phase favors formation of fine precipitates that are in thermodynamic equilibrium with the "matrix" bcc phase. The present systems do not offer the possibility of coherent precipitates, as the Laves phase is an fcc derivative and the primary disordered phases are bcc. Nevertheless, the present work suggests a reasoned approach for selecting constituent elements of a multi-principle element alloy, whereby some of the constituent binary phase diagrams show disordered solid solutions of a cubic phase and other constituent binary phase diagrams show ordered intermetallic phases derived from the same crystal structure symmetry.

The disordered bcc solid solution phase (A2-1) that is formed after solidification of the studied alloys is generally only stable at high temperatures in the equilibrium condition (see Fig. 11). At lower temperatures, it transforms into A2-2 and A3 phases in the NbTiVZr and $NbTiV_2Zr$ alloys, C15, A2-2 and A3 phases in the CrNbTiVZr alloy, and C15 and A3 phases in the CrNbTiZr alloy. While in the first three alloys the equilibrium A2-1 phase should not be present at temperatures below ~430 °C, it is predicted to be stable down to room temperature in the CrNbTiZr alloy. However, the experimental results do not show the presence of the A3 phase in the homogenized alloys. Moreover, the experimentally measured compositions of the bcc (A2) phases are typical to the compositions of these phases pre-

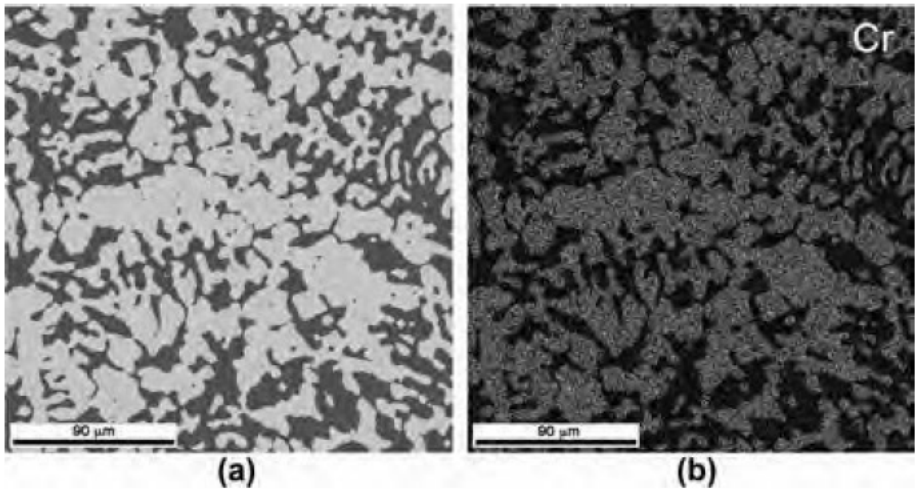

Fig. 9. EBSD/EDS maps of (a) bcc (dark) and fcc (light) phases and (b) distribution of Cr (regions with higher Cr concentrations are brighter) in the CrNbTiVZr alloy.

dicted at higher temperatures, e.g. 600 750 °C (compare the data in Tables 2 5 and 9). This analysis may indicate that cooling at the rate of 10 °C min ^{1} from a temperature of 1200 °C is too rapid to achieve the equilibrium conditions in the studied alloys, and the phases present at higher temperatures are retained, probably due to slow diffusion kinetics of the alloying elements. Indeed, sluggish diffusion of the alloying elements is one of the main features of high entropy alloys [2,3].

The experimental results show that none of the four refractory high entropy alloys has a single-phase crystal structure after high-temperature (1200 °C for 24 h) homogenization and slow cooling (10 °C min ^{1}). Although X-ray diffraction identifies only a single disordered bcc phase in NbTiVZr, SEM analysis shows the presence of fine, submicron-sized precipitates enriched with V and Zr-enriched regions surrounding these precipitates. Comparing these experimental results with the equilibrium phase diagram (Fig. 11a) and predicted compositions of equilibrium phases in the NbTiVZr alloy (Tables 9 and 10) suggests that the alloy matrix coincides with the non-transformed high-temperature A2-1 phase quenched from temperatures $\geqslant$726 °C, while dark secondary particles and bright regions surrounding these particles are likely coincide with the low-temperature A2-2 and A2-1 phases, respectively, formed in the two-phase range, below 700 °C.

An increased amount of vanadium in $NbTiV_2Zr$ results in the formation of three disordered bcc phases with different compositions and lattice parameters. The bcc1 (a 345.8 pm) is enriched with Zr and depleted of V, bcc2 (a 317.4 pm) is enriched with V and depleted of Zr, while the composition of the bcc3 (a 323.5 pm) is close to the average composition of the alloy. On the other hand, the thermodynamic model predicts only two equilibrium phases with bcc crystal structures, A2-1 and A2-2, which can be present together in equilibrium at temperatures from ~450 °C to 843 °C (see Fig. 11b). The A2-1 is depleted of V and enriched with Zr and the A2-2 is enriched with V and depleted of Zr in this temperature range. Above 843 °C, only the A2-1 phase is present and the composition of this phase is the same as the composition of the alloy. Comparison of these thermodynamic analysis results with the experimental results for the $NbTiV_2Zr$ alloy suggests that the bcc3 phase is a high-temperature A2-1 phase quenched from above 843 °C, while the bcc1 and bcc2 phases likely coincide with the lower temperature A2-1 and A2-2 phases, respectively, quenched from the two-phase range.

X-ray and microstructure analysis of the Cr-containing alloys, CrNbTiZr and CrNbTiVZr, show the presence of two phases, disordered bcc and ordered Laves, with distinct concentrations of alloying elements in both alloys. The CrNbTiZr contains 65% of bcc and 35% of Laves phases. In equilibrium, this phase proportion is present at temperatures of 650 800 °C (Fig. 11c), suggesting that the studied microstructure represents this temperature range. The CrNbTiVZr contains 39% of bcc and 61% of Laves phases. In accord with the thermodynamic modeling, this phase proportion cannot be achieved in equilibrium, as the maximum fraction of the Laves phase is predicted to be ~30% in this alloy. The compositions of the Laves phases observed in the CrNbTiZr and CrNbTiVZr are also different from those predicted by the model. Indeed, in accord with the thermodynamic analysis results, the Laves (C15) is essentially a binary phase, Cr_2Zr,

Table 5
Chemical composition (in at.%) of the CrNbTiVZr alloy constituents (see Fig. 8).

	Cr	Nb	Ti	V	Zr
Bright regions	4.1	31.6	33.1	12.8	18.4
Dark regions	29.4	16.1	9.7	22.2	22.7

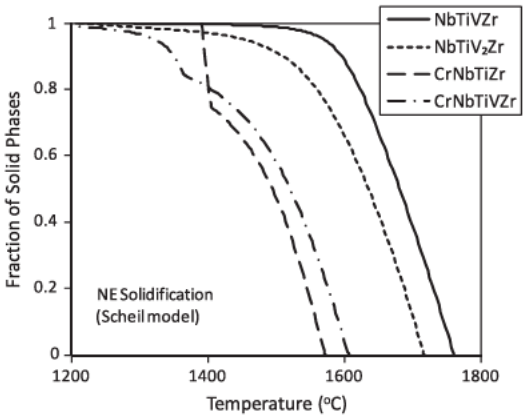

Fig. 10. The temperature dependence of the fraction of solid phases during non equilibrium solidification of CrNbTiZr, NbTiVZr, CrNbTiVZr and $NbTiV_2Zr$ alloys.

Table 6
Liquidus, T_L^{NE}, and solidus, T_S^{NE}, temperatures and fractions of solid phases in the four alloys after non equilibrium solidification (simulated results).

Alloy	T_L^{NE}, °C	T_S^{NE}, °C	Phase fraction		
			A2 1	A2 2	C15
NbTiVZr	1760	1207	0.999	0.001	0
$NbTiV_2Zr$	1717	1207	0.995	0.005	0
CrNbTiZr	1572	1391	0.912	0	0.088
CrNbTiVZr	1607	1103	0.95	0.005	0.045

Table 7
Average compositions (in at.%) of the phases in the studied alloys after non equilibrium solidification.

Phase ID	Element	NbTiVZr	$NbTiV_2Zr$	CrNbTiZr	CrNbTiVZr
bcc A2 1	Cr			21.0	17.9
	Nb	25.0	20.1	27.4	21.0
	Ti	25.0	20.1	27.2	21.0
	V	25.0	39.8		21.0
	Zr	25.0	20.1	24.4	19.1
bcc A2 2	Cr				8.0
	Nb	3.0	3.3		3.8
	Ti	3.9	3.9		1.2
	V	85.0	84.5		16.2
	Zr	8.1	8.2		70.8
Laves C15	Cr			66.4	65.9
	Nb			0.0	0.0
	Ti			2.8	0.8
	V				0.0
	Zr			30.9	33.3

consisting of 66.6 at.% Cr and 33.4 at.% Zr. The experimental results, however, show that this phase also contains other alloying elements. For example, in the CrNbTiZr, the Laves phase consists (approximately, in at.%) of 51Cr, 16Nb, 12Ti and 21Zr, which may indicate that some Cr is replaced with Nb and some Zr is substituted by Ti in this phase, which is now described as $(Cr,Nb)_2(Ti,Zr)$. In the CrNbTiVZr, the Laves phase consists of ~29Cr, 16Nb, 10Ti, 22V and 23Zr. This composition fulfills the formula $(Cr,Nb,V)_2(Ti,Zr)$. The capability for other alloying elements to substitute for Cr and Zr in the Cr_2Zr Laves phase allows an increasing volume fraction of this phase to be achieved. This analysis also highlights the limitations of the PanTi thermodynamic database used in this work. This database was developed by CompuTherm, LLC via extrapolation of the interaction parameters from the lower order constituent binary and ternary systems to higher order interactions [15]. Higher order (quaternary or quinary) interaction parameters should probably be used to match this thermodynamic database with the experimental data of the multi-component systems.

5. Summary and conclusions

1. High-hardness and low-density refractory multi-principal element alloys of the Cr Nb Ti V Zr system have been produced. The NbTiVZr, $NbTiV_2Zr$, CrNbTiZr and CrNbTiVZr alloys have densities of 6.52, 6.34, 6.67 and 6.57 g cm ^{3}, and Vickers microhardness values of 3.29, 2.99, 4.10 and 4.72 GPa, respectively. Disordered bcc solid solution phases are the major phases in these alloys, and Cr-containing alloys additionally contain an ordered Laves phase. Detailed information on the alloy phase compositions and crystal structures has been reported.
2. Non-equilibrium and equilibrium phase diagrams have been modeled for the studied alloys via extrapolation of the interaction parameters from the lower order constituent binary and ternary systems to higher order interactions. The models show that, after non-equilibrium solidification, the NbTiVZr and $NbTiV_2Zr$ alloys are essentially single-phase disordered bcc structures containing less than 1% of the secondary bcc phase. The disordered bcc phase also dominates (>91%) in the Cr-containing alloys, which additionally contain a Laves phase based on Cr and Zr.
3. Thermodynamic modeling of equilibrium phases shows that all the alloys have a single-phase bcc disordered structure (A2-1) just below the melting points. The temperature range of stability of this phase is greatest in the NbTiVZr alloy (down to 726 °C), followed by the $NbTiV_2Zr$ alloy (down to 843 °C). At lower temperatures, the A2-1 phase is predicted to partially transform in the secondary bcc (A2-2) and hexagonal phases in these alloys. The Cr-containing alloys also show the presence of a Laves phase below 1363 and 1234 °C for the CrNbTiZr and CrNbTiVZr alloys, respectively.
4. Comparing the thermodynamic modeling with experimental results shows that the volume fractions and compositions of the bcc phases identified in the studied alloys at room temperature approximately correspond to the equilibrium fractions and compositions of these phases at temperatures of ~600 750 °C. The present work thus suggests that a cooling rate of 10 °C min ^{1} to chill the alloys after homogenization treatment at

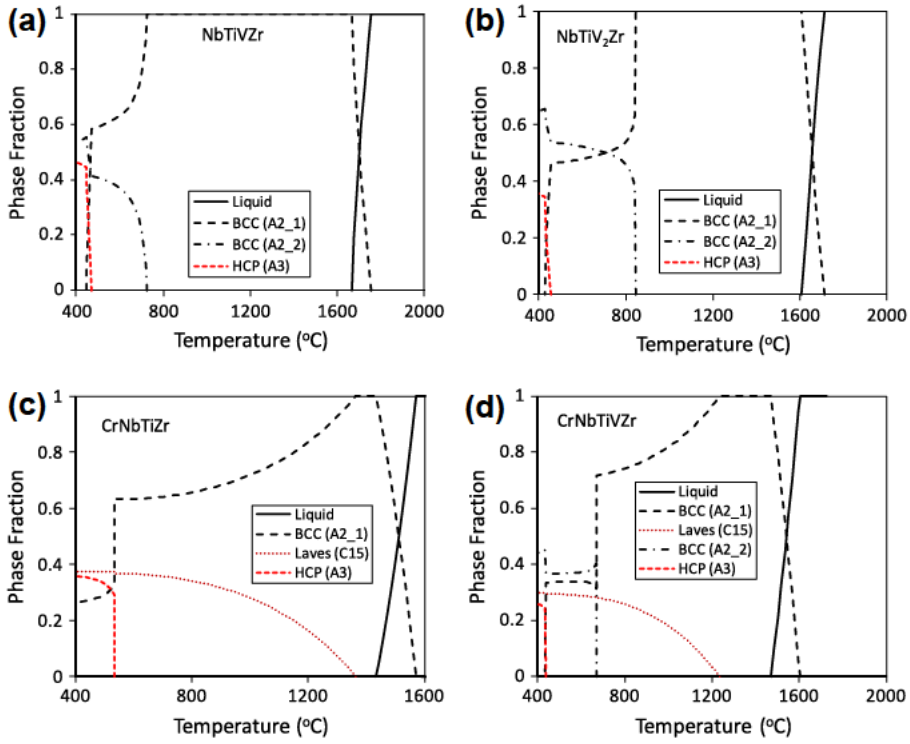

Fig. 11. Simulated equilibrium phase diagrams of the (a) NbTiVZr, (b) $NbTiV_2Zr$, (c) CrNbTiZr and (d) CrNbTiVZr alloys.

Table 8
Characteristic equilibrium phase transformation temperatures (in °C) and respective reaction equations in the studied alloys (simulated results).

Reaction equation	NbTiVZr	$NbTiV_2Zr$	CrNbTiZr	CrNbTiVZr
L → A2 1 (T_L)	1760	1717	1572	1607
L → A2 1 (T_S)	1668	1610	1432	1470
A2 1 → C15			1363	1234
A2 1 → A2 2	726	843		671
A2 1 → A3			535	
A2 1 → A2 2 + A3	471	456		
A2 1 → A2 2 + A3	446	426		
A2 1 → A2 2 + C15 + A3				440
A2 1 → A2 2 + C15 + A3				433

Table 9
Predicted volume fractions and compositions (in at.%) of equilibrium phases in the studied alloys at $T = 600$ °C.

	Fraction	Cr	Nb	Ti	V	Zr
NbTiVZr						
A2 1	0.636		13.6	32.4	18.5	35.5
A2 2	0.364		45.0	12.0	36.3	6.7
$NbTiV_2Zr$						
A2 1	0.477		7.6	31.4	23.0	38.0
A2 2	0.523		31.3	9.6	55.6	3.6
CrNbTiZr						
A2 1	0.633	0.9	39.5	39.5		20.2
C15	0.367	66.6		0.04		33.3
CrNbTiVZr						
A2 1	0.338	1.7	16.3	37.4	21.6	23.0
C15	0.288	66.6		0.03		33.4
A2 2	0.374	0.7	38.8	19.6	33.9	7.0

Table 10
Predicted volume fractions and compositions (in at.%) of equilibrium phases in the studied alloys at $T = 400$ °C.

	Fraction	Cr	Nb	Ti	V	Zr
NbTiVZr						
A2 2	0.535		46.5	6.1	46.3	1.1
A3	0.465		0.2	46.8	0.5	52.5
$NbTiV_2Zr$						
A2 2	0.646		30.9	6.8	61.6	0.7
A3	0.354		0.1	44.1	0.6	55.1
CrNbTiZr						
A2 1	0.264	0.0	93.9	3.8		2.3
C15	0.375	66.6		0.02		33.3
A3	0.361	0.0	0.5	66.5		33.0
CrNbTiVZr						
C15	0.300	66.6		0.02		33.3
A2 2	0.439	0.0	45.4	8.4	45.2	1.0
A3	0.261	0.0	0.3	62.5	0.6	36.6

1200 °C is too rapid to achieve equilibrium conditions below 600 750 °C. Thermodynamic databases based on the binary and ternary systems are able to predict correct trends, but are unable to accurately predict volume fractions and compositions of the Laves phases in the CrNbTiZr and CrNbTiVZr alloys.

5. Although the stabilization of disordered solid solutions is the defining feature of high entropy alloys, the present work identifies two systems where an ordered intermetallic phase is stable at room temperature and can be fully dissolved at high temperatures. This suggests a reasoned approach for developing high entropy alloys with both solid solution and ordered phases as candidate high-temperature structural materials.

Acknowledgements

This work was supported through the Air Force Research Laboratory Director's fund and through the Air Force on-site Contract No. FA8650-10-D-5226 conducted by UES, Inc., Dayton, Ohio.

References

[1] Yeh JW, Chen SK, Lin SJ, Gan JY, Chin TS, Shun TT. Adv Eng Mater 2004;6(5):299.
[2] Yeh JW. Ann Chim: Sci Mater 2006;31:633.
[3] Yeh JW, Chen YL, Lin SJ, Chen SK. Mater Sci Forum 2007;560:1.
[4] Zhang Y, Zhou YJ, Lin JP, Chen GL, Liaw PK. Adv Eng Mater 2008;10(6):534.
[5] Zhang Y, Yang X, Liaw PK. JOM 2012;64(7):830.
[6] Senkov ON, Wilks GB, Miracle DB, Chuang CP, Liaw PK. Intermetallics 2010;18:1758.
[7] Senkov ON, Wilks GB, Scott JM, Miracle DB. Intermetallics 2011;19:698.
[8] Senkov ON, Scott JM, Senkova SV, Miracle DB, Woodward CF. J Alloys Compd 2011;509:6043.
[9] Senkov ON, Scott JM, Senkova SV, Meisenkothen F, Miracle DB, Woodward CF. J Mater Sci 2012;47:4062.
[10] Senkov ON, Woodward CF. Mater Sci Eng A 2011;529:311.
[11] Senkov ON, Senkova SV, Dimiduk DM, Woodward C, Miracle DB. J Mater Sci 2012;47:6522.
[12] Senkov ON, Senkova SV, Miracle DB, Woodward CF. Mater Sci Eng A 2013, accepted for publication.
[13] Pandat 8.0. Phase diagram calculation software for multi component systems. Madison, WI: CompuTherm LLC; 2008.
[14] <http://www.aviationmetals.net/inconel.php>; 2012.
[15] Zhang C, Zhang F, Chen S, Cao W. JOM 2012;64(7):839.